Energy Dependence of Oxygen Isotope Exchange and Quenching in the $O(^1D) + CO_2$ Reaction: A Crossed Molecular Beam Study†

Mark J. Perri,‡ Annalise L. Van Wyngarden,‡ Jim J. Lin,§ Yuan T. Lee,§,|| and Kristie A. Boering*,‡,⊥

Department of Chemistry, University of California, Berkeley, California 94720, Institute of Atomic and Molecular Science, Academia Sinica, Taipei, Taiwan, Department of Chemistry, National Taiwan University, Taipei, Taiwan, Department of Earth and Planetary Science, University of California, Berkeley, California 94720, and Earth Science Division, Lawrence Berkeley National Laboratory, Berkeley, California 94720

Received: March 31, 2004; In Final Form: May 3, 2004

The dynamics of the $^{18}O(^1D) + {}^{44}CO_2$ oxygen isotope exchange reaction has been studied using a crossed molecular beam apparatus at collision energies of 4.2 and 7.7 kcal/mol. At both collision energies, two reaction channels are observed: isotope exchange in which quenching to $O(^3P)$ occurs and isotope exchange in which the product oxygen atom remains on the singlet surface. Electronic quenching of $O(^1D)$ is the major channel at both collision energies, accounting for 84% of isotope exchange at 4.2 kcal/mol and 67% at 7.7 kcal/mol. Both channels proceed via a CO_3* complex that is long-lived with respect to its rotational period. Combined with recent ab initio and statistical calculations by Mebel et al., the long complex lifetimes suggest that statistical isotope exchange occurs in the CO_3* complex (apart from zero-point energy isotope effects), although the existence of a small, dynamically driven unconventional isotope effect in this reaction cannot yet be ruled out. These new molecular-level details may help provide a more quantitative understanding of the heavy isotope enrichment in CO_2 observed in the stratosphere.

I. Introduction

Because of its importance in the atmosphere, the kinetics of $O(^1D)$ quenching by atoms and molecules has been studied extensively, including quenching by collision with CO_2 (R1).[1−3]

$$O(^1D) + CO_2\,(^1\Sigma) \rightarrow O(^3P) + CO_2(^1\Sigma) \qquad \Delta E = -46 \text{ kcal/mol} \quad \text{(R1)}$$

Quenching of $O(^1D)$ by CO_2 is a particularly interesting reaction because it is spin-forbidden but proceeds at an almost gas kinetic rate of 1.1×10^{-10} cm^3 s^{-1} at 298 K,[1−3] while reaction to form $CO+O_2$ ($^1\Sigma_g^+$, $^1\Delta_g$, $^3\Sigma_g^-$) proceeds at a rate of only 2.4×10^{-13} cm^3 s^{-1} for $O(^1D)$ produced by N_2O photolysis at 298 K.[4] Isotope labeling experiments in the 1960s, in which $O(^1D)$ was generated by photolysis of O_3,[5,6] N_2O,[7] NO_2,[8] and CO_2,[9] suggested that quenching of $O(^1D)$ by CO_2 involves the formation of a relatively long-lived intermediate, CO_3*, in which both isotope exchange and curve-crossing from the singlet to the triplet surface can occur. In particular, the experiment by Baulch and Breckenridge[9] led them to conclude that oxygen atom isotope exchange was nearly statistical in nature − that is, that the probability that a reactant oxygen atom was incorporated into the product CO_2 molecule was close to $^2/_3$. DeMore and Dede inferred a CO_3* lifetime of 1−10 ps from the pressure dependence of CO_3* formation at high pressures in the gas phase.[10] Beyond such inferences from kinetics and bulk isotope exchange studies, however, no direct information on the dynamics of isotope exchange and quenching in the $O(^1D) + CO_2$ reaction has been available until recently.

We recently reported results from a crossed molecular beam study of the $^{18}O(^1D) + {}^{44}CO_2$ oxygen isotope exchange reaction at a collision energy of 7.7 kcal/mol.[11] On the basis of the angular and kinetic energy distribution of the $^{46}CO_2$ products detected from this reaction, two different reaction channels were observed, both proceeding through a CO_3* complex that was long-lived with respect to its rotational period. Electronic quenching of $O(^1D)$ was the major channel (R2), accounting for 68% of all isotope exchange, while 32% of isotope exchange occurred without quenching (R3).

$$^{18}O(^1D) + {}^{44}CO_2 \rightarrow CO_3^* \rightarrow {}^{16}O(^3P) + {}^{46}CO_2 \quad \text{(R2)}$$

$$^{18}O(^1D) + {}^{44}CO_2 \rightarrow CO_3^* \rightarrow {}^{16}O(^1D) + {}^{46}CO_2 \quad \text{(R3)}$$

These results were the first experimental evidence that isotope exchange can occur through a long-lived CO_3* intermediate without subsequent crossing to the triplet surface.

The possibility of isotope exchange without quenching has yet to be considered in models of the unusual heavy oxygen isotope enrichments of ^{17}O and ^{18}O in stratospheric CO_2. Conventional equilibrium and kinetic isotope effects result in ^{17}O enrichments (relative to ^{16}O) that are half those for ^{18}O.[12,13] In contrast, the ^{17}O and ^{18}O isotopic compositions of stratospheric CO_2 are anomalous because the relative ^{17}O enrichments are a factor of 1.2−1.7 greater than the enrichments in ^{18}O.[14−20] Ozone in the atmosphere[19,21−24] and laboratory[25−32] also exhibits anomalous ^{17}O and ^{18}O enrichments due to unconventional isotope effects in the three-body recombination reaction (R4).[32−35]

† Part of the special issue "Richard Bersohn Memorial Issue".

* To whom correspondence should be addressed. E-mail: boering@cchem.berkeley.edu.

‡ Department of Chemistry, University of California, Berkeley.

§ Institute of Atomic and Molecular Science.

|| National Taiwan University.

⊥ Department of Earth and Planetary Science, University of California, Berkeley, and Lawrence Berkeley National Laboratory.

10.1021/jp0485845 CCC: $27.50
Published on Web 07/02/2004

$$O(^3P) + O_2 + M \rightarrow O_3^* + M \rightarrow O_3 + M \qquad (R4)$$

Marcus and co-workers[36−38] calculate that the anomalous isotope effect relevant for atmospheric ozone could result from a small non-RRKM effect leading to a lower density of states for symmetric isotopomers of O_3^* (e.g., $^{16}O^{16}O^{16}O$) than for the asymmetric isotopomers (e.g., $^{17}O^{16}O^{16}O$ and $^{18}O^{16}O^{16}O$) due to, for example, the absence of some anharmonic vibration−vibration and Coriolis rotation−vibration coupling terms due to symmetry restrictions for the symmetric species. On the basis of the ^{18}O isotope exchange laboratory studies between $O(^1D)$ and CO_2 discussed earlier, Yung et al. suggested that photolysis of anomalously enriched ozone in the stratosphere (R5)

$$O_3 + h\nu \rightarrow O(^1D) + O_2 \qquad (R5)$$

followed by statistical isotope exchange with CO_2 in R1 could explain the anomalous isotope enrichment in stratospheric CO_2.[39,40] To date, however, model predictions[40−42] of the ^{17}O and ^{18}O enrichments in CO_2 from the stratosphere and in bulk photochemistry laboratory experiments[42,43] have not reproduced observations sufficiently well to indicate that a molecular level understanding has been achieved, and no theory has yet been tested for the possibility of a dynamic, symmetry-driven anomalous isotope effect in the $CO_2 + O(^1D)$ reaction. Thus, with the molecular level information currently available, it is difficult to discern whether the discrepancies between models and measurements are due to lack of knowledge of ozone formation isotope effects (i.e., in the early studies noted), ozone photolysis isotope effects, conventional isotope effects in R1, possible anomalous isotope effects in R1 (e.g., due to the symmetry of CO_3^*), or the possibility of isotope exchange without quenching (R3) at energies relevant for the stratosphere (near 1.5 kcal/mol).[44] Resolving these unknowns is not only of fundamental chemical interest but may allow measurements of the anomalous isotopic composition of CO_2 to be used as both a unique tracer of stratospheric chemistry and transport on time scales of several years[20] and a means to quantify gross carbon fluxes to and from the biosphere on annual[45] to millennial[46,47] time scales.

To address some of the uncertainties in the molecular level details responsible for the isotope enrichments in stratospheric CO_2, and to obtain a more fundamental understanding of isotope exchange and quenching in the $CO_2 + O(^1D)$ reaction in general, we have modified our crossed-beam apparatus to employ a variable-speed $O(^1D)$ beam source. This modification allows the dynamics of the $CO_2 + O(^1D)$ reaction to be studied at collision energies as low as 4.2 kcal/mol, closer to typical stratospheric collision energies of 1.5 kcal/mol. In addition, coupled with theoretical calculations from Mebel et al.[48], these new results provide insight into the validity of the conclusion of Baulch and Breckenridge[9] from their bulk isotope exchange experiment that isotope exchange is statistical in the CO_3^* complex. Such new insight from the single collision environment of the crossed-beam apparatus may be useful because the Baulch and Breckenridge results may have been influenced by the very large isotope effects in the formation of ozone (R4) which were not recognized until the 1980s. Moreover, Baulch and Breckenridge also assumed that quenching occurred on every collision, which is likely not a valid assumption under their experimental conditions given our earlier crossed-beam results. Details of the crossed-beam experiment are described in section II, results are presented in section III, and results are then interpreted and compared with theoretical calculations by Mebel et al.[48] in section IV.

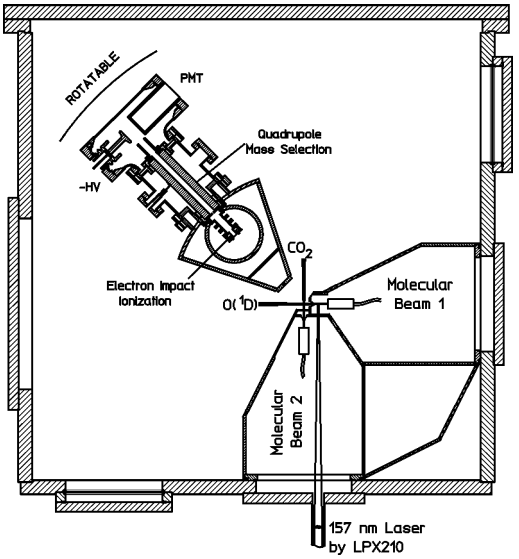

Figure 1. Schematic of the universal detector crossed molecular beam apparatus.

II. Experimental Section

A schematic of the universal crossed-beam apparatus used in this study, which has been described in detail elsewhere,[49] is shown in Figure 1. An atomic beam of 50% $^{18}O(^1D)$ and 50% $^{18}O(^3P)$ was produced by photolysis of $^{36}O_2$ at 157 nm. The $^{36}O_2$ had an isotopic purity greater than 95% as verified by mass spectrometry. Using isotopically labeled ^{18}O as the atomic beam and detecting $^{46}CO_2$ avoided background from the reactant $^{44}CO_2$ beam (in which $^{46}CO_2$ was present in its natural abundance at 0.4%) and ensured all products detected had undergone isotopic exchange.

The O_2 beam was produced from a tuned pulsed valve (General Valve) with a rise time of approximately 50 μs. A backing pressure of approximately 10 psi was used. The photolysis laser (Lambda Physik LPX 210 F_2 laser), with a power of 60 mJ per pulse at a 50 Hz repetition rate, was focused with a spherical-cylindrical MgF_2 lens to a spot size of 3 mm $\times$ 4 mm, saturating the O_2 transition. The $O(^1D)$ speed is determined by the initial velocity of the O_2 in the horizontal direction (into the chamber) and the energy released from photolysis. In the earlier crossed-beam experiment,[11] the pulsed valve was fixed perpendicular to the reaction plane to reduce background O_2 gas in the main chamber. To produce slower $O(^1D)$ speeds in the experiment reported here, the pulsed valve nozzle was angled backward away from the main chamber, which gave the O_2 beam an initial negative horizontal momentum (Figure 2). When the laser photolyzed the O_2, $O(^1D)$ was produced with less forward momentum into the main chamber than if the pulsed valve was at its original perpendicular angle. Geometric constraints on placing the nozzle in the source chamber limited the speeds achievable to between 1540 and 2160 m/s with a speed ratio of approximately 8. With this redesigned pulsed valve arrangement, there was not enough room to place a skimmer after the photolysis region. Therefore, two pieces of sheet metal were cut to form a "V" to collimate the $O(^1D)$ beam in the vertical direction (see Figure 2). The $O(^1D)$ exit aperture also served to collimate the beam. As a result, the angular divergence of the $O(^1D)$ beam in the horizontal plane increased slightly, from $\pm 4°$ in the previous experiment to $\pm 4.5°$.

To form a molecular beam of CO_2, a mixture of 33% CO_2 (99.99%) in Ar (99.999%) was used; this also served to increase

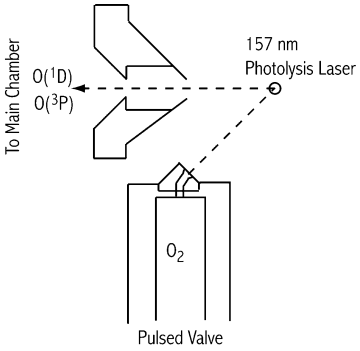

Figure 2. Schematic of the modifications to the slow $O(^1D)$ source used to access collision energies down to 4.2 kcal/mol.

the speed ratio of the beam. A low backing pressure between 6 and 16 psig was used to reduce the formation of clusters. A tuned pulsed valve (General Valve) similar to that for the O_2 source was used along with a 1.5 mm diameter skimmer. The average CO_2 beam speed was 620 ± 5 m/s with a speed ratio of 11 and an angular divergence of ±3°. With the fixed CO_2 speed and variable $O(^1D)$ speeds, the collision energy could be varied between 4.2 and 7.7 kcal/mol. For this experiment, the two extreme collision energies were used.

After both beams emerge from the source chambers, they pass through a copper cold plate cooled to 20 K by a closed cycle helium cryocooler. This cold plate condenses stray CO_2 that would otherwise become background in the main chamber and thus dramatically increases the signal-to-noise ratio. After the CO_2 and $O(^1D)$ beams cross, the neutral products travel 247 mm to the detector where they are ionized by electron impact. Product ions resulting from isotope exchange ($^{46}CO_2$) are mass selected by a quadrupole mass filter and pass through to a Daly detector, resulting in time-of-flight spectra which are acquired by a multichannel scaler with a 1 μs bin size. To determine the angular dependence of the reaction, the detector is attached to the top flange of the main chamber and can be rotated about the beam crossing point from −35° to 125°, with the $O(^1D)$ beam defined as 0°. The full range of the detector was not used in this experiment due to the high background generated close to the beam directions. The angles studied range from 0° to 70° with additional measurements at 115° and 117°. Isotope exchange between ^{18}O atoms and $^{44}CO_2$ on the cold plate generates a large background $^{46}CO_2$ signal close to 0°; however, it is possible to collect data at 0° because at that angle molecules escaping the cold plate will not intercept the detector. At angles near 90°, the normal isotopic abundance of $^{46}CO_2$ in the beam gives rise to a high background. Despite these limitations, the laboratory angles measured cover almost the entire range of center of mass angles relevant for this study.

To extract center-of-mass product speed and angular information as well as the branching ratio between the two isotope exchange channels from the raw data, computer simulations were performed. Initial estimates for the center-of-mass product kinetic energy distribution, $P(E)$, and the center-of-mass product angular distribution, $P(\theta)$, were input into an iterative forward-convolution computer program. Laboratory-frame time-of-flight spectra were generated on the basis of the input distributions for $P(E)$ and $P(\theta)$, molecular beam parameters, and machine dimensions. The resulting TOF spectra were then compared with the experimental data, which were rebinned to 3 μs to improve the signal-to-noise ratio. The values of $P(E)$ and $P(\theta)$ for each channel were then iteratively adjusted to achieve a satisfactory fit to the TOF data.

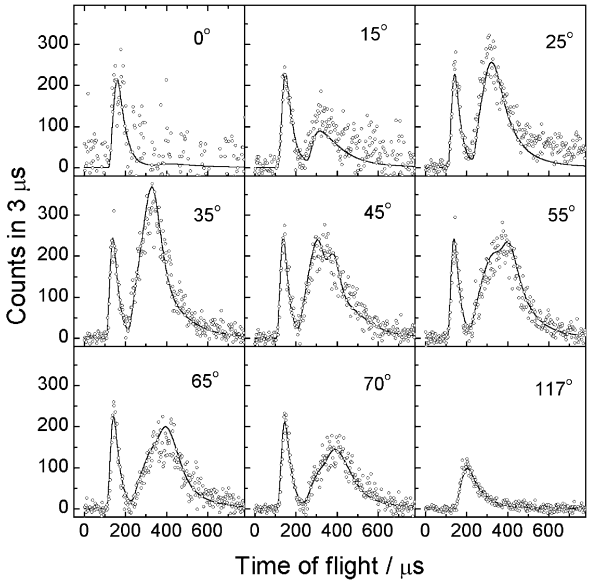

Figure 3. Time-of-flight spectra at mass 46 ($^{18}O^{12}C^{16}O$) at a collision energy of 4.2 kcal/mol for nine different laboratory angles. The open circles represent the experimental data (corrected for $^{46}CO_2$ at natural abundance in the CO_2 beam; see text); solid lines are the simulated results.

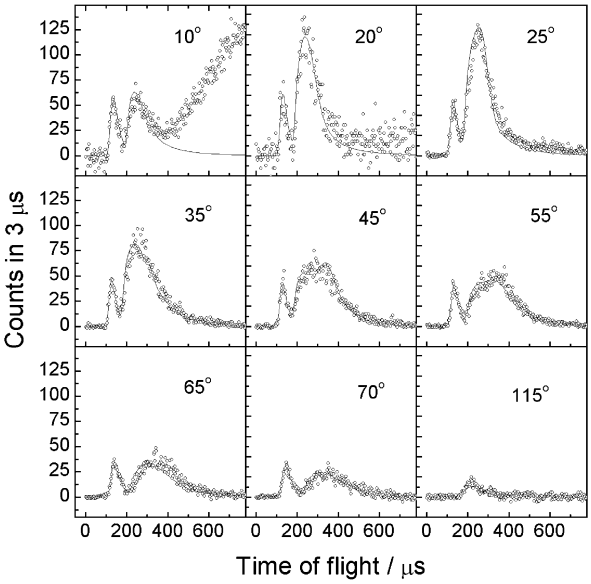

Figure 4. Time-of-flight spectra at mass 46 ($^{18}O^{12}C^{16}O$) at a collision energy of 7.7 kcal/mol for nine different laboratory angles. The open circles represent the experimental data (corrected for $^{46}CO_2$ at natural abundance in the CO_2 beam; see text); solid lines are the simulated results. The increase in signal at a lab angle of 10° is due to isotope exchange between ^{18}O and $^{44}CO_2$ on the cold plate (see text).

III. Results

Time-of-flight data (symbols) and results for the simulated TOF data (lines) for $^{46}CO_2$ products are shown in Figure 3 for the lower collision energy of 4.2 kcal/mol. There are two distinct peaks, a fast peak with an average flight time of 140 μs at a laboratory angle of 45° and a slower, broader peak centered at approximately 320 μs at 45°. Data for the higher collision energy of 7.7 kcal/mol are shown in Figure 4 and are virtually identical to the earlier published results[11] at this same energy. Two distinct peaks are also seen, one at 130 μs at a laboratory angle of 45° and one at approximately 280 μs at 45°. Note that $^{46}CO_2$ background generated by surface reactions on the cold plate is apparent at long times at the laboratory angle of 10° but does

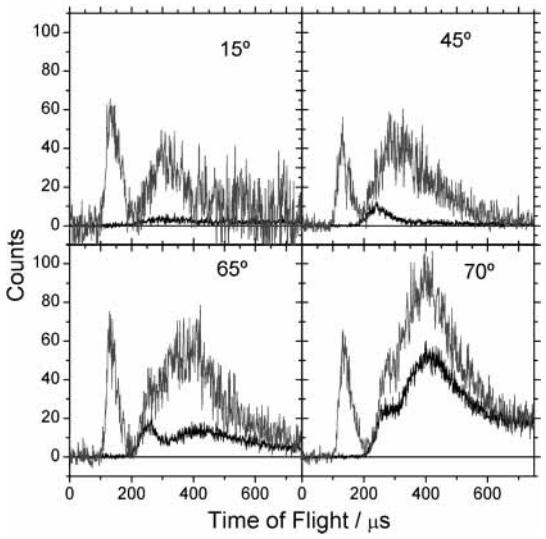

Figure 5. Correction for the natural abundance of $^{46}CO_2$ present in the reactant $^{44}CO_2$ beam. The gray line represents the raw time-of-flight data, while the black line represents the contribution from $^{46}CO_2$ in the reactant beam (see text).

not affect the data analysis because it is well separated from the data of interest. We also note that, in an improvement over the analysis in our earlier work, a correction has been made for interference due to the natural abundance of $^{46}CO_2$ (0.4%) in the reactant CO_2 beam. A portion of this small amount of $^{46}CO_2$ undergoes elastic and inelastic scattering with the O(^{1}D) beam and appears as an extra peak at long times. Corrections were applied to both the 4.2 and the 7.7 kcal/mol TOF data in Figures 3 and 4 by measuring the scattering of the $^{44}CO_2$ reactant beam and then scaling the results to the natural abundance of $^{46}CO_2$. The uncorrected TOF data along with the scaled $^{46}CO_2$ background for four angles from the 4.2 kcal/mol data are shown in Figure 5. The correction is negligible at small laboratory angles but grows to a significant portion of the slow peak at large laboratory angles. This correction does not significantly affect the simulated $P(E)$ and $P(\theta)$ distributions but does make the TOF data easier to fit.

The results do not depend on the backing pressure of the CO_2 beam, thus ensuring that both the fast and the slow peaks are from collisions of CO_2 monomers with oxygen atoms and not CO_2 dimers or clusters. Because only mass 46 is detected and a small correction for $^{46}CO_2$ in the reactant beam due to natural background has been made, both the fast and the slow channels observed must correspond to isotope exchange. Moreover, because the barrier for any possible isotope exchange between O(^{3}P) and CO_2 is predicted to be approximately 36 kcal/mol,[48,50] and the earlier bulk isotope exchange experiments showed no exchange between O(^{3}P) and CO_2,[5,7] both peaks observed have been assigned to two different O(^{1}D) + CO_2 channels.

The product kinetic energy and center-of-mass angular distributions resulting from the simulations for both channels at both collision energies are shown in Figures 6 and 7, respectively. The derived values for $P(E)$ and $P(\theta)$ for the two channels are graphed as product velocity flux diagrams ($d\sigma/(du \sin \vartheta d\vartheta)$) in contour plots with the Newton diagram superimposed (Figure 8) and in three-dimensional surface plots (Figure 9).

At both collision energies, the slow channel corresponds to the inner channel in Figure 8a and 8b and has a maximum translational energy release equal to the collision energy. Thus, we attribute this channel at both collision energies studied to

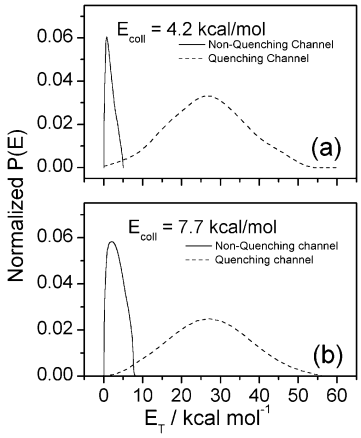

Figure 6. Product kinetic energy distributions, $P(E)$, for the collisions energies of (a) 4.2 and (b) 7.7 kcal/mol which best simulate the TOF experimental data in Figures 3 and 4, respectively. The probabilities have been normalized to the branching ratios for the individual channels.

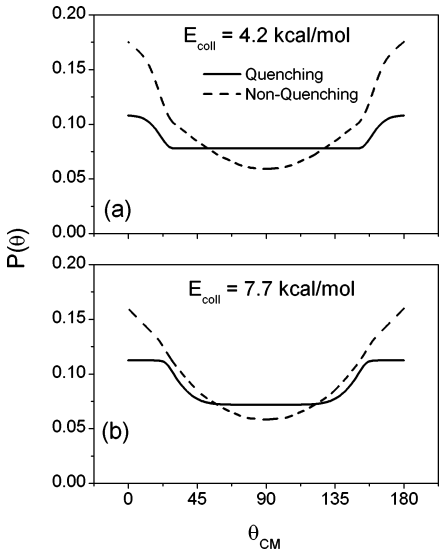

Figure 7. Product angular distributions, $P(\theta)$, for the collisions energies of (a) 4.2 and (b) 7.7 kcal/mol which best simulate the TOF experimental data in Figures 3 and 4, respectively. The solid curves correspond to the quenching channel, and the dashed curves correspond to the nonquenching channel.

TABLE 1: Branching Ratios and Product Translational Energies

collision energy (kcal mol^{-1})	channel	branching ratio	$\langle E_{trans} \rangle$ (kcal mol^{-1})	f_{int}[a]
4.2	quenching	84%	26.0	0.48
	nonquenching	16%	1.8	0.57
7.7	quenching	67%	27.4	0.49
	nonquenching	33%	3.3	0.57

[a] $f_{int} = E_{int}/(E_{trans} + E_{int})$.

oxygen isotope exchange between O(^{1}D) and CO_2 without quenching − that is, isotope exchange on the singlet surface (R3). The fast channel observed at both collision energies has a maximum translational energy release much greater than that of the collision energy and is therefore attributed to isotope exchange with quenching (R2). Both the fast and the slow channels have similar product angular distributions that are forward−backward symmetric, indicating that they proceed through complexes that are long-lived with respect to rotation (see Figures 8 and 9). The main difference between the results at the two collision energies is the relative intensity of the

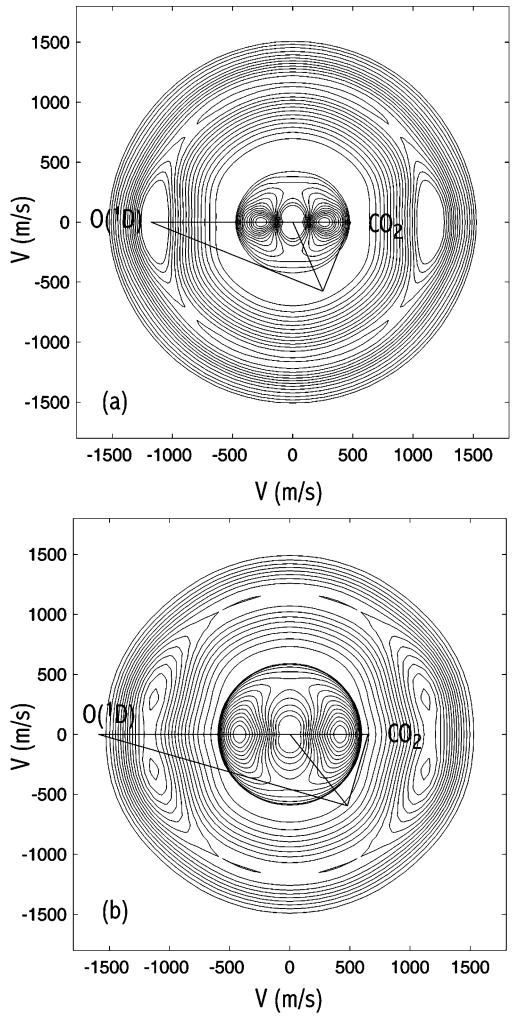

Figure 8. Product velocity flux contour diagrams derived from the simulated $P(E)$ and $P(\theta)$ distributions for $^{46}CO_2$ products at a collision energy of (a) 4.2 and (b) 7.7 kcal/mol. The quenching channel corresponds to the fast products far from the center-of-mass (center of figure). The nonquenching channel is the inner slower product channel seen. Because the nonquenching channel is less than 20% of the intensity of the quenching channel, the contours for each channel are not on the same scale.

quenching (R2) and "nonquenching" channels (R3), which we will refer to as the branching ratio. The difference in branching ratios as a function of collision energy can be clearly seen in the relative heights of the product flux diagrams (Figure 9). At 7.7 kcal/mol, the nonquenching channel accounts for 33% of the observed isotope exchange. At 4.2 kcal/mol, this percentage has decreased to 16%, demonstrating a decreased importance of the nonquenching channel at lower collision energies.

A summary of the branching ratios and translational energy release for the quenching and nonquenching channels at both collision energies is shown in Table 1. For the lower collision energy, the average translational energy release, $\langle E_t \rangle$, is 1.8 kcal/mol for the nonquenching channel and 26.0 kcal/mol for the quenching channel. Of the total energy available for reaction, this leaves 57% and 48% for internal excitation of the $^{46}CO_2$ product for the nonquenching and quenching channels, respectively. The higher collision energy results are similar, with $\langle E_t \rangle$ equal to 3.3 and 27.4 kcal/mol for the nonquenching and quenching channels, respectively. This leaves 57% and 49% of the total energy for internal excitation of CO_2, identical to the results at the lower collision energy. These values are consistent with those obtained in a flow tube study where a higher collision energy of 13.0 kcal/mol was used; by measuring the product $O(^3P_2)$ Doppler profile at 130.2 nm, it was found that $49 \pm 3\%$ of the available energy was deposited into the product CO_2.[51]

IV. Discussion

The results presented here extend the investigation of the dynamics of oxygen isotope exchange in the $CO_2 + O(^1D)$ reaction from a collision energy of 7.7 kcal/mol down to 4.2 kcal/mol. At both energies, isotope exchange occurs via a long-lived CO_3* complex, as indicated by the forward−backward symmetry of the scattering of product CO_2. No evidence for a direct isotope exchange mechanism is observed at either collision energy. The magnitude of the branching ratio between the channel for isotope exchange with quenching (R2) and without quenching (R3), however, is a strong function of collision energy. The relative importance of the quenching channel increases with decreasing collision energy. This result is examined more quantitatively by Mebel et al.[48] in which high-level ab initio calculations of energies, molecular parameters, and spin−orbit coupling constants are combined with RRKM theory and the theory of radiationless transitions to calculate the $O(^3P)/O(^1D)$ product branching ratio as a function of energy. Their calculated values compare favorably with the experimental values presented here and do show the expected increase in the quenching channel branching ratio with decreasing collision energy. In their calculations, this effect is shown to be due to a sharp decrease in the rate of decomposition of CO_3* on the singlet surface to $O(^1D) + CO_2$ as the collision energy is lowered.

The ab initio calculations of Mebel et al. also highlight the importance of the symmetry of the CO_3* complex itself in the isotope exchange process. Although IR spectroscopy of CO_3 formed and trapped in solid CO_2 and Ar matrixes showed that the C_{2v} structure is the most stable structure at low temperatures,[6,52,53] the C_{2v} and D_{3h} isomers of CO_3* can rapidly interconvert on the $^1A_1$ surface in the crossed-beam experiment because these structures have approximately the same energy and the barrier between them is only 4.4 kcal/mol.[48] Thus, facile interconversion of the C_{2v} and D_{3h} isomers, coupled with a long CO_3* lifetime in which intramolecular vibrational energy redistribution (IVR) may be complete, could therefore lead to statistical isotope exchange in the CO_3* complex (apart from small zero-point energy isotope effects; see below). Indeed, the calculations of Mebel et al., which assume complete IVR in their use of RRKM theory, do predict that the attacking $O(^1D)$ atom has a probability of being incorporated into the product CO_2 molecule of $^2/_3$.[48]

Overall, then, the dynamics of the $CO_2 + O(^1D)$ reaction investigated here, combined with the theoretical calculations of Mebel et al., are broadly consistent with earlier isotope exchange experiments and inferences from kinetics studies which suggested that isotope exchange and quenching proceed via a long-lived complex and that isotope exchange in the CO_3* complex is roughly statistical. Several insights have arisen from this new work, however, which may be critical for understanding and modeling the oxygen isotopic composition of stratospheric CO_2. First, Mebel et al. calculate the small degree to which isotope exchange in the CO_3* complex departs from pure statistics for $^{44}CO_2$ versus $^{46}CO_2$. These deviations are due to differences in zero-point energies and the numbers and densities of states involved. For example, they calculate that the ratio for the probability of a ^{16}O atom versus an ^{18}O atom being ejected from a CO_3* complex is just slightly greater than the statistical value of 2 for both channels: 2.014 for the quenching channel (R2)

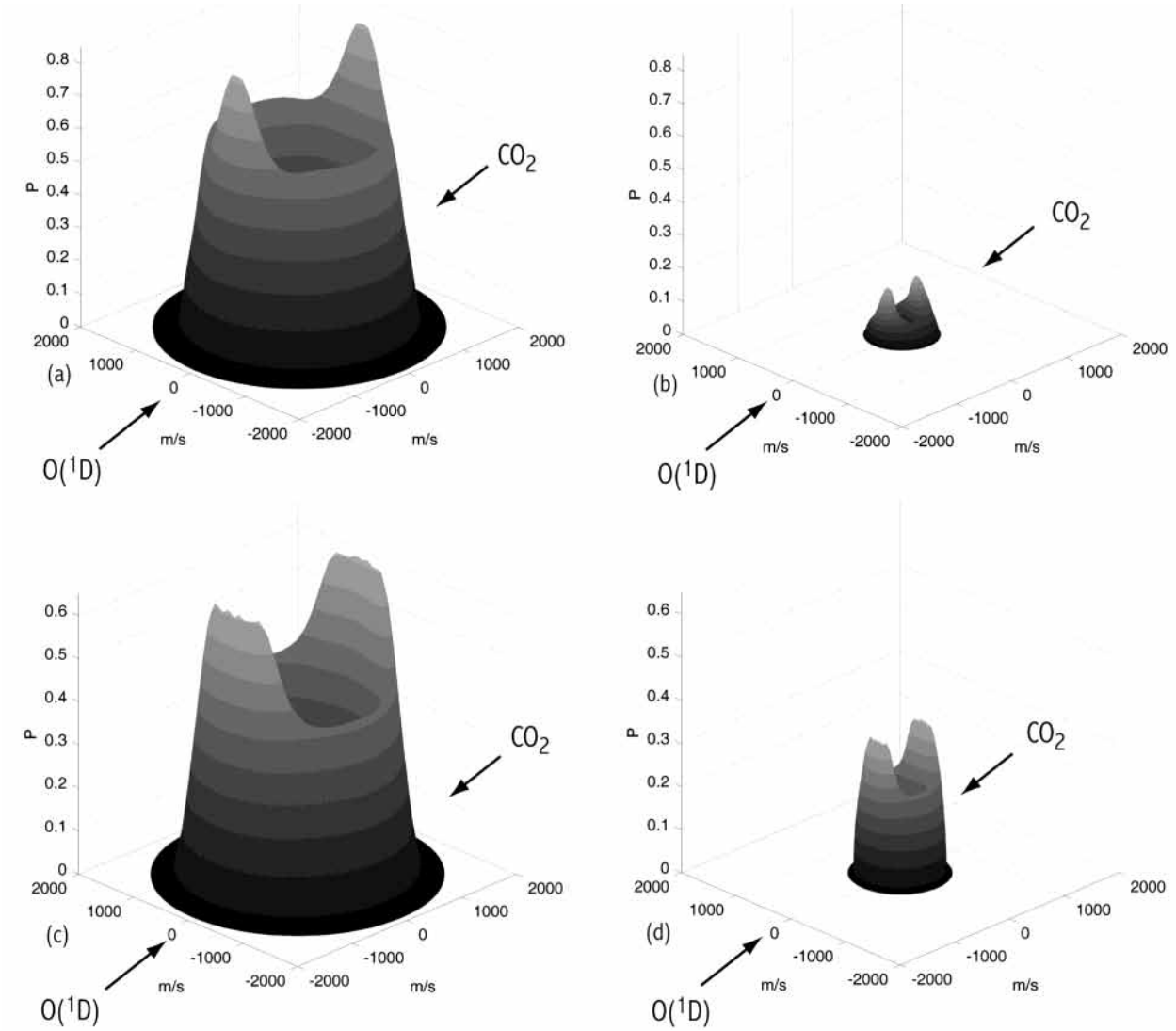

Figure 9. The 3D center-of-mass product velocity flux diagram from the simulated $P(E)$ and $P(\theta)$ distributions for $^{46}CO_2$ products. (a,b) Quenching and nonquenching channels for a collision energy of 4.2 kcal/mol, respectively. (c,d) Quenching and nonquenching channels for a collision energy of 7.7 kcal/mol. The probabilities have been normalized by the branching ratio of each channel.

and 2.052 for the singlet channel (R3) at 4.2 kcal/mol (see their Table 6). Importantly, these small departures from a statistical value of 2 depend on collision energy; the energy dependence of the departures is different for the $O(^1D)$ versus $O(^3P)$ product channels; and the differences are largest at the lowest collision energies.[48] The latter result may be particularly relevant for the stratosphere, where the $CO_2 + O(^1D)$ collision energies are on the order of 1.5 kcal/mol.[44] Both the existence of a mechanism for isotope exchange without quenching and inclusion of high-level calculations of isotope effects in the $CO_2 + O(^1D)$ reaction and their energy dependence have yet to be investigated in atmospheric models of the isotopic composition of stratospheric CO_2 and in photochemical kinetics modeling of laboratory experiments involving isotope exchange between ozone and CO_2.

These combined experimental and theoretical results also point to additional studies that can be pursued to probe the origin (or origins) of the anomalous enrichments of ^{17}O and ^{18}O in stratospheric CO_2. As noted earlier, there remains some controversy over whether the formation or decomposition of the CO_3* complex could exhibit an anomalous isotope effect similar to that for O_3* complexes that Marcus and co-workers suggest is a non-RRKM effect resulting from dynamical differences between symmetric and asymmetric O_3 isotopomers (i.e., the "eta effect," one of two unconventional isotope effects in Marcus' treatment of the ozone recombination reaction).[36] The calculations of Mebel et al. suggest that the rates of isomerization between the C_{2v} and D_{3h} structures of the CO_3 complex are slightly higher than the RRKM applicability limit − that is, that they may be faster than rates for IVR.[48] Therefore, the possibility of a dynamic effect ultimately resulting in unconventional isotope effects for ^{17}O and ^{18}O in CO_2 − perhaps driven by subtle symmetry effects − cannot be ruled out without further study. A more complete theoretical understanding of the "eta" isotope effect for O_3* may ultimately point the way toward understanding whether a similar symmetry-driven isotope effect might exist for CO_3* and/or whether the "eta" isotope effect could result from collisional effects which would not be relevant for the $CO_2 + O(^1D)$ reaction. (Note that Babikov et al.[54−56] performed full quantum scattering calculations for the second unconventional isotope effect in ozone formation, which is mass-dependent, and not for the so-called "eta effect" most relevant for the atmosphere.) In addition, the results presented here and by Mebel et al.[48] can be incorporated into models of the isotopic composition of stratospheric CO_2 and of laboratory experiments involving the irradiation of O_3/CO_2 mixtures to test whether the anomalous enrichment in ^{17}O and ^{18}O in CO_2 can be explained solely by photochemical transfer from anomalously

fractionated ozone via $O(^1D)$ or whether an additional anomalous isotope effect in R2 or R3 is required.

V. Summary

In summary, the dynamics of isotope exchange between $O(^1D)$ and CO_2 has been studied using a crossed-beam apparatus at two collision energies: 4.2 and 7.7 kcal/mol. Two isotope exchange channels are observed − a fast channel corresponding to electronic quenching, yielding $O(^3P)$ and CO_2 products, and a slow channel without electronic quenching, yielding $O(^1D)$ and CO_2 products. The nonquenching isotope exchange channel, which accounts for 16% of all isotope exchange at a collision energy of 4.2 kcal/mol, is predicted by Mebel et al.[48] to decrease to approximately 5% at stratospheric collision energies. The symmetry of the CO_2 product angular distribution at both collision energies studied demonstrates that the CO_3* complex formed is long-lived with respect to rotation and is consistent with a statistical probability of incorporation of the incoming $O(^1D)$ into the final CO_2 of $^2/_3$. Theoretical calculations by Mebel et al.[48] support this interpretation and provide additional insights into small deviations from the pure statistical probability of $^2/_3$ due to conventional isotope effects. The possibility of a small, unconventional isotope effect contributing to anomalous ^{17}O and ^{18}O enrichments in CO_2 which has undergone isotope exchange with $O(^1D)$, however, cannot yet be ruled out. These new molecular level insights and details can now be incorporated into atmospheric and photochemical kinetics models to determine their impact on predictions of the heavy oxygen isotope enrichments of CO_2 in the stratosphere and in laboratory experiments.

Acknowledgment. This research was supported by the U.S. National Science Foundation Atmospheric Chemistry Program (ATM-0096504), by Academia Sinica, Taiwan, by a National Science Foundation Predoctoral Fellowship (A.L.V.), and by the David and Lucile Packard Foundation (K.A.B.). We are thankful to Prof. A. M. Mebel for insightful comments and stimulating discussion.

References and Notes

(1) Davidson, J. A.; Sadowski, C. M.; Schiff, H. I.; Streit, G. E.; Howard, C. J.; Jennings, D. A.; Schmeltekopf, A. L. *J. Chem. Phys.* **1976**, *64*, 57.
(2) Streit, G. E.; Howard, C. J.; Schmeltekopf, A. L.; Davidson, J. A.; Schiff, H. I. *J. Chem. Phys.* **1976**, *65*, 4761.
(3) Sander, S. P.; Finlayson-Pitts, B. J.; Friedl, R. R.; Golden, D. M.; Huie, R. E.; Kolb, C. E.; Kurylo, M. J.; Molina, M. J.; Moortgat, G. K.; Orkin, V. L.; Ravishankara, A. R. Jet Propulsion Laboratory, JPL Publication 02-25, Pasadena, CA, 2002.
(4) Sedlacek, A. J.; Harding, D. R.; Weston, R. E.; Kreutz, T. G.; Flynn, G. W. *J. Chem. Phys.* **1989**, *91*, 7550.
(5) Katakis, D.; Taube, H. *J. Chem. Phys.* **1962**, *36*, 416.
(6) Weissberger, E.; Breckenridge, W. H.; Taube, H. *J. Chem. Phys.* **1967**, *47*, 1764.
(7) Yamazaki, H.; Cvetanovic, R. J. *J. Chem. Phys.* **1964**, *40*, 582.
(8) Preston, K. F.; Cvetanovic, R. J. *J. Chem. Phys.* **1966**, *45*, 2888.
(9) Baulch, D. L.; Breckenridge, W. H. *Trans. Faraday Soc.* **1966**, *62*, 2768.
(10) Demore, W. B.; Dede, C. *J. Phys. Chem.* **1970**, *74*, 2621.
(11) Perri, M. J.; Van Wyngarden, A. L.; Boering, K. A.; Lin, J. J.; Lee, Y. T. *J. Chem. Phys.* **2003**, *119*, 8213.
(12) Thiemens, M. H. *Science* **1999**, *283*, 341.
(13) Weston, R. E. *Chem. Rev.* **1999**, *99*, 2115.
(14) Gamo, T.; Tsutsumi, M.; Sakai, H.; Nakazawa, T.; Tanaka, M.; Honda, H.; Kubo, H.; Itoh, T. *Tellus B* **1989**, *41*, 127.
(15) Thiemens, M. H.; Jackson, T.; Mauersberger, K.; Schueler, B.; Morton, J. *Geophys. Res. Lett.* **1991**, *18*, 669.
(16) Thiemens, M. H.; Jackson, T.; Zipf, E. C.; Erdman, P. W.; Vanegmond, C. *Science* **1995**, *270*, 969.
(17) Thiemens, M. H.; Jackson, T. L.; Brenninkmeijer, C. A. M. *Geophys. Res. Lett.* **1995**, *22*, 255.
(18) Alexander, B.; Vollmer, M. K.; Jackson, T.; Weiss, R. F.; Thiemens, M. H. *Geophys. Res. Lett.* **2001**, *28*, 4103.
(19) Lammerzahl, P.; Rockmann, T.; Brenninkmeijer, C. A. M.; Krankowsky, D.; Mauersberger, K. *Geophys. Res. Lett.* **2002**, *29*, doi: 10.1029/2001GL014343.
(20) Boering, K. A.; Jackson, T.; Hoag, K. J.; Cole, A. S.; Perri, M. J.; Thiemens, M.; Atlas, E. *Geophys. Res. Lett.* **2004**, *31*, L03109, doi: 10.1029/2003GL018451.
(21) Mauersberger, K. *Geophys. Res. Lett.* **1981**, *8*, 935.
(22) Mauersberger, K. *Geophys. Res. Lett.* **1987**, *14*, 80.
(23) Schueler, B.; Morton, J.; Mauersberger, K. *Geophys. Res. Lett.* **1990**, *17*, 1295.
(24) Krankowsky, D.; Lammerzahl, P.; Mauersberger, K. *Geophys. Res. Lett.* **2000**, *27*, 2593.
(25) Thiemens, M. H.; Gupta, S.; Chang, S. *Meteoritics* **1983**, *18*, 408.
(26) Heidenreich, J. E.; Thiemens, M. H. *J. Chem. Phys.* **1986**, *84*, 2129.
(27) Thiemens, M. H.; Jackson, T. *Geophys. Res. Lett.* **1987**, *14*, 624.
(28) Morton, J.; Barnes, J.; Schueler, B.; Mauersberger, K. *J. Geophys. Res., D: Atmos.* **1990**, *95*, 901.
(29) Mauersberger, K.; Morton, J.; Schueler, B. *Abstr. Pap. − Am. Chem. Soc.* **1991**, *201*, 294.
(30) Mauersberger, K.; Morton, J.; Schueler, B.; Stehr, J.; Anderson, S. M. *Geophys. Res. Lett.* **1993**, *20*, 1031.
(31) Anderson, S. M.; Hulsebusch, D.; Mauersberger, K. *J. Chem. Phys.* **1997**, *107*, 5385.
(32) Mauersberger, K.; Erbacher, B.; Krankowsky, D.; Gunther, J.; Nickel, R. *Science* **1999**, *283*, 370.
(33) Janssen, C.; Guenther, J.; Krankowsky, D.; Mauersberger, K. *J. Chem. Phys.* **1999**, *111*, 7179.
(34) Janssen, C.; Guenther, J.; Krankowsky, D.; Mauersberger, K. *J. Chem. Phys.* **2000**, *112*, 11109.
(35) Janssen, C.; Guenther, J.; Mauersberger, K.; Krankowsky, D. *Phys. Chem. Chem. Phys.* **2001**, *3*, 4718.
(36) Gao, Y. Q.; Marcus, R. A. *Science* **2001**, *293*, 259.
(37) Gao, Y. Q.; Marcus, R. A. *J. Chem. Phys.* **2002**, *116*, 5913.
(38) Gao, Y. Q.; Chen, W. C.; Marcus, R. A. *J. Chem. Phys.* **2002**, *117*, 1536.
(39) Yung, Y. L.; Demore, W. B.; Pinto, J. P. *Geophys. Res. Lett.* **1991**, *18*, 13.
(40) Yung, Y. L.; Lee, A. Y. T.; Irion, F. W.; DeMore, W. B.; Wen, J. *J. Geophys. Res., D: Atmos.* **1997**, *102*, 10857.
(41) Barth, V.; Zahn, A. *J. Geophys. Res., D: Atmos.* **1997**, *102*, 12995.
(42) Johnston, J. C.; Rockmann, T.; Brenninkmeijer, C. A. M. *J. Geophys. Res., D: Atmos.* **2000**, *105*, 15213.
(43) Wen, J.; Thiemens, M. H. *J. Geophys. Res., D: Atmos.* **1993**, *98*, 12801.
(44) Takahashi, K.; Taniguchi, N.; Sato, Y.; Matsumi, Y. *J. Geophys. Res., D: Atmos.* **2002**, *107*, doi: 10.1029/2001JD001270.
(45) Hoag, K. J.; Boering, K. A.; Still, C. J.; Fung, I. Y.; Randerson, J. T. *EOS Trans. Am. Geophys. Union* **2002**, *83*, Fall Meet. Suppl., Abstract B71A-0707.
(46) Luz, B.; Barkan, E.; Bender, M. L.; Thiemens, M. H.; Boering, K. A. *Nature* **1999**, *400*, 547.
(47) Blunier, T.; Barnett, B.; Bender, M. L.; Hendricks, M. B. *Global Biogeochem. Cycles* **2002**, *16*, doi: 10.1029/2001GV001460.
(48) Mebel, A. M.; Hayashi, M.; Kislov, V. V.; Lin, S. H. *J. Phys. Chem. A* **2004**, *108*, 7983.
(49) Lin, J. J.; Hwang, D. W.; Harich, S.; Lee, Y. T.; Yang, X. M. *Rev. Sci. Instrum.* **1998**, *69*, 1642.
(50) Froese, R. D. J.; Goddard, J. D. *J. Phys. Chem.* **1993**, *97*, 7484.
(51) Matsumi, Y.; Inagaki, Y.; Morley, G. P.; Kawasaki, M. *J. Chem. Phys.* **1994**, *100*, 315.
(52) Moll, N. G.; Clutter, D. R.; Thompson, W. E. *J. Chem. Phys.* **1966**, *45*, 4469.
(53) Jacox, M. E.; Milligan, D. E. *J. Chem. Phys.* **1971**, *54*, 919.
(54) Babikov, D.; Kendrick, B. K.; Walker, R. B.; Pack, R. T.; Fleurat-Lesard, P.; Schinke, R. *J. Chem. Phys.* **2003**, *119*, 2577.
(55) Babikov, D.; Kendrick, B. K.; Walker, R. B.; Pack, R. T.; Fleurat-Lesard, P.; Schinke, R. *J. Chem. Phys.* **2003**, *118*, 6298.
(56) Babikov, D.; Kendrick, B. K.; Walker, R. B.; Schinke, R.; Pack, R. T. *Chem. Phys. Lett.* **2003**, *372*, 686.